Role of tidal mixing on ocean exchange through the Strait of Hormuz

Mohammed Salim[1,2], Subeesh M. P.[1,3,4], Jeffery Scott[5], Hajoon Song[6,7], John Marshall[5], and Maryam R. Al Shehhi[1]*

[1]Department of Civil Infrastructure and Environmental Engineering, Khalifa University of Science and Technology, Abu Dhabi, United Arab Emirates
[2]Department of Meteorology, University of Reading, UK.
[3]MARUM – Center for Marine Environmental Science, University of Bremen, Bremen, Germany
[4]Institute of Environmental Physics, University of Bremen, Bremen, Germany
[5]Earth, Atmospheric and Planetary Science Department, Massachusetts Institute of Technology, 77 Massachusetts Ave., Cambridge, MA 02139, USA.
[6]Department of Atmospheric Sciences, Yonsei University, Seoul, Korea
[7]Division of Environmental Science & Engineering, Pohang University of Science and Technology, Pohang, Republic of Korea

Key Points:

- Simulations show that the presence of tides and its associated mixing suppresses exchange through the Strait of Hormuz.
- Bottom water flowing out through the Strait is fresher and warmer in the presence of tides.
- Mixing reduces the lateral density gradient between the inner Gulf and outer Ocean, reducing exchange.

Corresponding author: Maryam R. Al Shehhi, maryamr.alshehhi@ku.ac.ae

Abstract

We investigate the influence of tides on the exchange of water between the Arabian Gulf and the Sea of Oman through the Strait of Hormuz using a high-resolution numerical model. Two numerical simulations are contrasted, one with and one without tidal forcing. We find that tides suppress exchange through the Strait, by ∼20% in the annual mean, being largest in the summer (∼30%) and diminishing in the winter (∼13%). Tides enhance the parameterised shear-driven vertical mixing inside the Gulf and Strait, mixing warm, relatively fresh surface waters downward thus reducing the density of bottom waters flowing outwards. This reduces the lateral difference of density between Gulf and Sea of Oman and hence the exchange through the Strait. Maximum reductions occur in summer when both the vertical stratification and mixing is the largest.

Plain Language Summary

In a modeling study we explore how tides affect the exchange of water between the Arabian Gulf and the Sea of Oman through the Strait of Hormuz. We find that tides reduce the exchange by roughly 20% in the annual mean, the effect being greatest and reaching 30% in the summer. Tides enhance the mixing of warm, fresh surface waters downwards in the water column, reducing the density of bottom waters inside the Gulf. This results in a diminution of the gross density difference between the Gulf and the Sea of Oman and hence reduces the exchange. The effect is most pronounced in the summer when Gulf waters are the most stratified and mixing the greatest. We conclude that the realism of ocean models of the Gulf will be greatly enhanced if they explicitly represent tides and their associated mixing.

1 Introduction

The Arabian Gulf (AG) is a shallow basin located between the northern boundary of the Arabian Peninsula and Iran, Figure. 1a) . Its ocean is one of the most saline in the world (Figure. 1b,c). Due to its arid climate, evaporation exceeds freshwater input, and is compensated by a net surface inflow through the narrow Strait of Hormuz (SH) (Alosairi et al., 2020; Privett, 1959; Johns et al., 2003; Xue & Eltahir, 2015). In compensation, warm, saline and oxygenated waters residing at shallow depths of the AG, exit lower down the water column through the Strait (Figure. 1b). These spread at intermediate depths into the Arabian Sea and the Bay of Bengal, ultimately significantly affecting the hydrography of the north Indian Ocean (Jain et al., 2017; Sheehan et al., 2020; Pous et al., 2004a, 2004b). AG water plays a significant role in the ventilation of the oxygen minimum zone of the Arabian Sea (McCreary et al., 2013). Understanding the mechanism behind AG water outflow through the SH is thus of great importance. An improved understanding of water mass transport between the AG and Sea of Oman may also better inform efforts to preserve the marine environments of the region.

Many modelling and observational studies have addressed the circulation of the AG and the characteristics of the water mass exchange through the SH (Thoppil & Hogan, 2010a; Johns et al., 2003; Pous et al., 2004a, 2015; Lorenz et al., 2021; Kämpf & Sadrinasab, 2006; Reynolds, 1993a). The circulation of the AG is broadly cyclonic and the SH plays an important role in restricting the exchange between the Gulf and Sea of Oman (Reynolds, 1993a; Emery, 1956; Brewer & Dyrssen, 1985; Hunter, 1983; Reynolds, 1993a; Chao et al., 1992; Johns et al., 2003). These studies have explored the various processes at work that control exchange. Swift and Bower (2003) suggest that changes in sea surface slope between the Sea of Oman and the AG is the primary driving force of exchange on synoptic time scales. Thoppil and Hogan (2010a) and Vasou et al. (2020) noted that such short timescale variability is set by the local winds. According to Vasou et al. (2020), short-term variability (2 to 5 day) in transport shows a quasi-barotropic pattern affecting mostly the upper layers. On longer time scales (seasonal to interannual), exchange

through the SH is thought to be controlled by the horizontal density gradient between the inner Gulf and the Sea of Oman (Pous et al., 2015; Chao et al., 1992; Yao & Johns, 2010; Thoppil & Hogan, 2010a; Kämpf & Sadrinasab, 2006).

Studies have suggested that mixing within the AG is associated with strong tidal currents, topographic features and eddy activity (Lorenz et al., 2021; Swift & Bower, 2003). However, previous studies of watermass exchange through the SH have disregarded the role of tides in the time-mean general circulation, assuming that its affect is small when averaged over periods longer than a few tidal cycles (Pous et al., 2012; Hughes & Hunter, 1979). The one exception of which we are aware is the recent study of Campos et al. (2022) who find, as here, that inclusion of tides significantly reduces exchange. However, they did not explore underlying mechanisms. Studies in different straits indeed find that diapycnal mixing and residual currents induced by tides can play a significant role in water mass modification and the large-scale circulation (Koch-Larrouy et al., 2007; Nagai & Hibiya, 2015) by affecting inflow and outflow (Farmer & Armi, 1986; Naranjo et al., 2014; Sannino et al., 2004, 2015; Kurogi & Hasumi, 2019). In this study, then, we follow on from the work of Campos et al. (2022) and focus in on the underlying mechanisms at work. We employ a high resolution 3D model of the AG previously reported in Al-Shehhi et al. (2021) and contrast solutions with and without tidal forcing.

2 A high resolution model of the Arabian Gulf based on MITgcm

We make use of a high-resolution configuration of the MITgcm (Marshall et al., 1997) deployed for the Arabian Gulf as described in Al-Shehhi et al. (2021). The MITgcm has been extensively used in studies of tides, internal tides, and residual currents in coastal waters in the presence of complex topographies and geometries — see, for example, (Sannino et al., 2015; Wang et al., 2015). The model is configured for the AG and Sea of Oman (23.2°N to 30.7°N and 47.3°E to 62.3°E) as shown in Figure 1a. It is driven by meteorological forcing at its upper surface, from tides prescribed at its open-ocean lateral boundaries and by river inflow along the coasts. It has a high horizontal spatial resolution of approximately 2.5 km and 83 vertical levels ranging from 1 m in thickness at the surface to ∼200 m at the bottom out in the Sea of Oman. More details can be found in Al-Shehhi et al. (2021). A high-resolution bathymetry data set derived from (Smith & Sandwell, 1997) is used with a resolution of 3 km. The model is adjusted so that evaporation over the AG is compensated by freshwater fluxes from the lateral boundary (E-P-R; where E is Evaporation, P is Precipitation and R River run-off). A standard configuration of the nonlocal K-profile parameterization (KPP) (Large et al., 1994, 1997) is used to parameterize ocean turbulent mixing.

The temperature, salinity and velocity components for initial and lateral boundary conditions are obtained from a $1/48^0$ MITgcm global model simulations known as LLC4320 (Rocha et al., 2016). The model was forced at the surface by 6-h European Centre for Medium-Range Weather Forecasts (ECMWF) atmospheric operational model analysis at 0.148^0 resolution (∼15 km). A custom monthly river freshwater outflow dataset (capturing the discharge of the Shatt Al-Arab, Mand, Hindijan, and Hilieh rivers) is also included obtained from Large and Nurser (2001) and as described in Al-Shehhi et al. (2021).

The amplitude and phase of seven tidal constituents (M2, S2, N2, K2, K1, O1 and P1) obtained from the Arabian Sea regional barotropic tidal model, OSU Tidal Inversion Software (OTIS) (Egbert et al., 1994; Egbert & Erofeeva, 2002), are prescribed along the open boundaries. The model's fidelity in capturing tidal patterns and amplitudes is assessed in the supplementary material, where it is compared with observations from tide gauges. The spatial distribution of the four major tidal constituents is also presented there. The model effectively captures tidal features, consistent with previous studies (Mashayekh Poul et al., 2016; Pous et al., 2012; Hyder et al., 2013; Madah & Gharbi, 2022). The M2 tide is the most dominant constituent in the Gulf and Sea of Oman, followed by K1, S2, and

O1. The co-tidal maps shows two amphidromic points for semi-diurnal tides: one in the southeastern Gulf near Abu Dhabi and another in the southwestern Gulf. Additionally, a diurnal tide amphidromic point is located in the south-central Gulf off Bahrain's coast (see supplementary). Here we focus on the impact of those tides on mixing and the general circulation, in particular exchange through the SH.

To study the effect of tides on the general circulation within the Gulf, we designed two numerical experiments driven by: (i) atmospheric forcing with no tides and (ii) both tides and atmospheric forcing. The model is integrated for the year 2012 in a repeating cycle. The model is run on for 6 years with repeating surface forcing and boundary conditions and the final two years are used in analysis. We also carried out a multi-year calculation including tidal and atmospheric forcing from 2003 to 2018 to ensure that interannual variability does not affect our conclusion. We find that interannual variability in exchange through the Strait is indeed small compared to the difference of transport due to the inclusion of tidal processes.

3 Comparing simulations with and without tides

3.1 The role of tides in the exchange through the Strait of Hormuz

We analysed our most realistic simulation which included tidal forcing (hereafter "tidal run") and compared it to an additional calculation in which the tidal forcing is removed (hereafter "non-tidal run"). The monthly volume transport through the cross-section CS (marked in Figure 1a) are computed by integrating positive (outflow) and negative (inflow) values across the transect: see Figure 2g. In both tidal and non-tidal simulations, the volume transport shows similar seasonal variation peaking during late winter and again in summer. However, the magnitude of transport differs between them, with a yearly-averaged 20% reduction in the tidal case: the average outflow (inflow) is 0.278 (.285) Sv and 0.357 (0.352) Sv for tidal and non-tidal runs respectively. Seasonal-average values show that the volume transport is reduced by 30% in summer and 13% in winter. The standard deviation of volume transport across the strait due to interannual atmospheric forcing is also indicated in Figure 2g. It is evidently small compared to the difference between tidal and non-tidal transport.

The annual mean transport estimated from our tidal run is closer to observational estimates than in the absence of tides. The annual mean volume transport through the Strait inferred from mooring observations (Johns et al., 2003) is $\sim$0.23$\pm$ 0.04 Sv (inflow) and $\sim$0.21$\pm$ 0.05 Sv (outflow). Thus, including tides reduces the tendency of our model to over-estimate the exchange between the AG and the Sea of Oman. Other modelling studies driven by tides from open boundaries are also broadly consistent with observed estimates of inflow (outflow), e.g. Pous et al. (2015): 0.203 (0.194), Pous et al. (2004b): 0.21 (0.17) and Vasou et al. (2020): 0.22(0.15). That said, our results suggest that including tidal forcing is critical to obtaining a realistic representation of exchange through the Strait.

3.2 Circulation driven with tides and atmospheric forcing

We examined a vertical cross section of the model's currents through the Strait to understand the change in volume transport in tidal and non-tidal simulations. The currents are averaged for winter (DJF) and summer (JJA) and the zonal component of the current velocity is shown (see Figure 2 a-d) along the line CS. Positive values show outflow (red shading) and negative values inflow (blue). The inflow occurs through the northern half of the Strait and outflow through the southern half. In winter, the inflow is largely barotropic, but the outflow occurs predominantly at depths below 60m, particularly in the non-tidal run where bottom currents peak at order 30 cm/s. Without tides the outflow is weak in the southern half of the Strait at depths shallower than 60m, even ex-

hibiting slight inflow along the southern coast (largely absent from the tidal run). In summer, however, differences are more pronounced. Without tides, inflow remains fairly uniform in the vertical, while outflow is largest at depth. However, with tides both inflow and outflow are largest in the top 40m of the Strait. Note that the bottom-intensified outflow remains fairly constant throughout the year, implying that the summer exchange peak is largely associated with the barotropic component in the absence of tides, but is surface intensified in the presence of tides.

To further compare tidal and non-tidal runs, we show the difference in bottom currents in a plan view of the AG (Figure 2 e-f). Tidal forcing suppresses currents at depth, extending out to the Sea of Oman through the SH. We also analyzed the larger-scale circulation to determine whether tidal influences are restricted to the SH or whether there are basin-wide changes — see the depth-averaged and surface currents plotted in Supplementary Fig. S6 & S7. It is found that the tide has impact throughout the Gulf, and particularly along its northern coast. The largest difference between tidal and non-tidal runs is found in the Gulf, to the west of Siri Island close to the SH, where depth average speed differences reach $21cms^{-1}$ and $25cms^{-1}$ in winter and summer respectively. The maximum residual current speeds in the SH during summer are $20cms^{-1}$ and $33cms^{-1}$ for tidal and non-tidal runs respectively, during winter $29cms^{-1}$ and $32cms^{-1}$. In addition to the effect of tides on current speeds, tidal forcing significantly affects flow patterns. The north-westward flowing Iranian Coastal Current (ICC), which is associated with density gradients between the AG and the Sea of Oman (Swift & Bower, 2003; Thoppil & Hogan, 2010b), is prominent during both winter and summer in the non-tidal run. The weaker ICC in winter is attributed to the reduced density gradient between the Sea of Oman and the AG due to winter cooling effects. The addition of tidal forcing weakens and modifies the ICC in all seasons. The summer and winter circulation patterns (see Supplementary Figure S5) both show that the tide induces a large change in circulation. The addition of tides expands the gyre and its strength is significantly reduced in winter. The major tidal modifications on circulation patterns occur within the Gulf, predominantly to the north where the bathymetry is deeper and most sharply changing.

3.3 Effect of tides on hydrography

The above results show that tidal forcing significantly modifies the basin wide circulation, with substantial reduction in deep currents in the SH. As noted in previous studies, the density gradient between the AG and the Sea of Oman is the dominant force driving seasonal circulation in the Gulf (Yao & Johns, 2010; Kämpf & Sadrinasab, 2006; Thoppil & Hogan, 2010b). Any change in this gradient may affect the basin-wide circulation and exchange through the Strait. In order to understand whether tidal forcing has any role in hydrographic structure, and thereby circulation and exchange, we analyzed the temperature and salinity distributions in tidal and non-tidal simulations.

We first compared seasonal-means of temperature, salinity and density with historical observations from the Master Oceanographic Observations Dataset (MOODS) (Alessi et al., 1999) which spans the 1940-1990 period. Al-Shehhi et al. (2021) compared the seasonal-average hydrography obtained from the tidal run used in this study with the same MOODS observations. Here we extend this comparison to the non-tidal simulation. We take 18 boxes along the center of the AG from its north-west corner to the Sea of Oman, and horizontally average the hydrography from the non-tidal run for summer (see Fig. 3) and winter (see supplementary Fig. S8). The boundaries of the boxes (see Fig. 1a) are defined following Swift and Bower (2003). Comparing tidal and non-tidal runs with observations (upper rows of Fig. 3 & S8), we see that both have similar biases, specifically a too warm and fresh bias toward the surface (i.e., too light) and too cold and salty at depth (i.e., too dense). However, these biases are less pronounced in the tidal simulation. This can be seen most clearly when we compare the density (right column): the

tidal run remains modestly too light at the surface (i.e. remains too warm and fresh), but exhibits minimal bias at depth. The bottom water density is significantly reduced in the tidal run. During winter, the densities in both the tidal and non-tidal simulations are closer to observations. The non-tidal run shows a difference of 1 kgm^{-3} with observation in summer, whereas the bias is 0.3 kgm^{-3} in the presence of tides. In summary, summer biases in temperature, salinity and density are considerably reduced in the presence of tides.

The simulated spatial distribution of bottom temperature, salinity and density differences during DJF and JJA is presented in the supplementary materials (see Fig S9 in the Supplementary section). Tidal forcing is felt across the entire basin in both AG and SH with a strong influence during the summer (JJA) months. The box-average difference between tidal and nontidal runs over the AG ($47.3^oE : 56^oE, 23.2^oN : 30.7^oN$) is found to be 0.25^oC and 0.43^oC during winter and summer respectively. The AG bottom water is freshened by 0.26 (0.5)psu in winter (summer) in the presence of tides. Waters on the southern coast of the AG (UAE) are more saline, and dense water to the south is more saline than dense water to the north. A similar observation was made by Swift and Bower (2003). The decrease in salinity and increase in temperature decreases the bottom density basin wide. The AG is strongly stratified by temperature during summer, with a weaker salinity increase with depth (Al-Shehhi et al., 2021). In the presence of tides, bottom temperatures in the SH ($56^oE : 57^oE, 25.8^oN : 27.5^oN$) exhibit a larger increase of 0.6^oC in winter and 0.9^oC in summer than without tides. The salinity in the presence of tides is decreased at the bottom. In summary, tidal-induced mixing acts to cool and increase salinity at the surface, and warm and freshen at depth.

3.4 Vertical Mixing

To infer the vertical mixing due to tides, we compared the model-derived vertical (diapycnal) mixing in the two simulations. The depth-averaged vertical mixing (Kv, Fig, 4. a&b) is distinctly elevated relative to without tides in summer in the AG. The vertical profile of mixing, Fig. 4c, shows a higher Kv with tides between depths of 20m and 110m in summer and 60m to 100m in winter. In the SH, the Kv with tides is elevated by a factor of 4 and 1.5 in summer and winter, respectively. This suggests that the vertical mixing of tracers is significantly enhanced in the presence of tides. Fig. 4 also shows the ratio between the vertical mixing (tide and notide) for winter and summer. In summer tidal mixing is found throughout the domain, i.e., it is more significant in the presence of stratified waters and so summer water masses are more influenced by the tides than in winter. The buoyancy frequency ($N = \sqrt{-\frac{g}{\rho}\frac{d\rho}{dz}}$, where ρ is the potential density) also documents the weakening of the stratification with tides (Fig. 4). The spatial distribution shows that the difference between the two simulations (tide - notide) is generally negative everywhere in the AG and SH. The maximum weakening of the stratification occurs during the summer period.

To study the impact of tidal mixing on horizontal density gradients we estimated the average density between two boxes, one inside the AG (average of Boxes 10,11 & 12) and a second box outside the SH, in the Sea of Oman (average of Boxes 17 & 18). Fig. 4 (e) shows the vertical profiles of this difference in the summer (JJA) and winter (DJF) seasons, comparing tidal and non-tidal simulations. In the presence of tides we see a notable reduction of this difference in the summer, particularly between depths of 40m and 90m. In contrast this effect is considerably weaker in winter. The mixing of lighter waters downwards due to tides is thus seen to decrease the horizontal density difference. In winter, the tide has little effect on these gradients. The reduced density gradient between the AG and Sea of Oman in the presence of tides is likely an important factor in the significant suppression of deep water outflow in summer.

4 Summary and Conclusions

We have investigated the impact of tides on the exchange between the AG and the Sea of Oman through the Strait of Hormuz (SH) by comparing high resolution numerical experiments with and without tidal forcing. The reliability of the tides simulated in the model is assessed — as set out in the supplimentary material — by comparing the model with time series observations from coastal tide gauges and current meters. We find that the tide modifies basin-wide circulation and impacts the properties and volume flux of deep water outflow through the SH (Fig. 2. f&g). The outflow (and compensating inflow) is suppressed in the presence of tides by 20% in the annual mean, by 30% in summer and 13% in winter (Fig. 2a). This broadly confirms the recent study of Campos et al. (2022) who used a different model.

Earlier studies have shown that barotropic tides can induce residual currents in the Gulf due to the non-linear interaction of large-amplitude tidal currents with bathymetry: the M2 residual itself can exceed $0.15ms^{-1}$ in the AG — see Poul et al. (2016). Some large-scale circulation changes found in our model may thus be associated with such residuals. However, the primary reason for large-scale changes, we believe, is due to the presence of enhanced vertical mixing induced by the tides.

We find that mean bottom currents are significantly suppressed in the presence of tides due to the modification of the hydrographic structure inside the Gulf. The deep waters in the SH are warmed by 0.7^oC and freshened by 0.62 psu (average of summer and winter months) when tides are included (see supplementary Fig. S8), indicative of enhanced downward vertical mixing of lighter surface waters. The increase in bottom temperature is larger in summer than winter, and is associated with stronger summertime tidal mixing. The reduction of basin-wide stratification also confirms elevated vertical mixing rates with tides. Enhanced shear-driven mixing, especially in summer, reduces the density of the bottom water within the AG, reduces the lateral density between the AG and Oman Sea and, concomitantly, the rate of lateral exchange. The effect is weaker in the winter than in the summer. Indeed the AG is well mixed in winter and so the role of tides in setting deep water outflow is much reduced.

The spatial distribution of vertical mixing shows large values in the vicinity of topography features such as small seamounts and shelf-slope regions (Fig. 4). Tide-topography interaction and generation of internal tides is one of the important processes of enhancing mixing. The greater stratification in summer, together with the presence of many topographic features, facilitates strong internal tides and enhanced mixing. The bottom water modification due to tide-topography interaction also occurs elsewhere in the ocean — see, e.g., the Jithin and Francis (2020) study of warm bottom waters in the Andaman Sea of the north-eastern Indian Ocean. Recently (Kurogi & Hasumi, 2019) also noted the tidal suppression of through-flow in a narrow Strait of Seto Inland Sea, Japan. Our key result should be contrasted with, for example, Naranjo et al. (2014) who found outflow increases significantly in the Strait of Gibralter by 28% to 33% annually in the presence of tides.

The AG is known for its markedly distinct winter and summer characteristics, primarily due to significant seasonal shifts in temperature and salinity (T/S properties). Despite these marked variations in T/S properties, they are not prominently reflected in the exchange rates through the SH (Johns et al., 1998; Swift & Bower, 2003). We find that tidal suppression in summer is the major factor maintaining a steady exchange. Our study suggests that both winter and summer water masses respond differently to tides. The tide significantly suppresses the through-flow of stratified summer water and hence controls the density driven circulation/exchange.

Climate change projections show that the AG may undergo substantial warming with perhaps adverse effects on marine ecosystems (Field & Barros, 2014; Paparella et

al., 2022). The summer SST of AG could increase by perhaps 4^oC or so by 2100 (Noori et al., 2019), leading to an increase in stratification as the upper ocean warms. It would be interesting to know whether increased stratification due to this warming enhances the baroclinic tide and its associated mixing or reduces mixing due to the increased stratification. Whatever happens, future increased warming may affect exchange flows between the AG and the Sea of Oman due to the modulation of mixing from tides/internal tides acting on seasonally stratified Gulf waters.

Data Availability Statement

The Model (MIT-gcm) setup with compile-time and run-time parameters can be found at `http://wwwcvs.mitgcm.org/viewvc/MITgcm/MITgcm_contrib/llc_hires/llc_4320/`.The Master Oceanographic Observations Dataset (MOODS), utilized in this study, originates from Alessi et al. (1999). Tidal amplitude and phase data, derived from tide gauge observations, were obtained from Pous et al. (2012), with the original source being the International Hydrographic Office. Current data from mooring stations, as cited in Reynolds (1993b), are publicly available at NOAA National Oceanographic Data Center `https://www.nodc.noaa.gov/archive/arc0001/9600082/1.2/data/`.

Acknowledgments
We acknowledges Khalifa University for its generous financial support and HPC Khalifa University for the Model run. H. Song is grateful for the support by National Research Foundation of Korea (NRF) Grant (NRF-2022R1A2C1009792 and 2018R1A5A1024958) and the Research Program for the carbon cycle between oceans, land, and atmosphere of the NRF funded by the Ministry of Science and ICT (2022M3I6A108599012). JM received support from the Physical Oceanography Program of NASA. We used pyFERRET, MATLAB and GMT extensively for the data analysis and generating figures.

References

Alessi, C. A., Hunt, H. D., & Bower, A. S. (1999). *Hydrographic data from the us naval oceanographic office: Persian Gulf, southern red sea, and arabian sea 1923-1996.* (Tech. Rep.). WOODS HOLE OCEANOGRAPHIC INSTITUTION MA.

Alosairi, Y., Alsulaiman, N., Rashed, A., & Al-Houti, D. (2020). World record extreme sea surface temperatures in the northwestern Arabian/persian gulf verified by in situ measurements. *Marine Pollution Bulletin*, *161*. doi: 10.1016/j.marpolbul.2020.111766

Al-Shehhi, M. R., Song, H., Scott, J., & Marshall, J. (2021). Water mass transformation and overturning circulation in the Arabian Gulf. *Journal of Physical Oceanography*, *51*(11), 3513–3527.

Brewer, P. G., & Dyrssen, D. (1985). Chemical oceanography of the Persian Gulf. *Progress in oceanography*, *14*, 41–55.

Campos, E. J., Kjerfve, B., Cavalcante, G., Vieira, F., & Abouleish, M. (2022). Water exchange across the strait of hormuz. effects of tides and rivers runoff. *Regional Studies in Marine Science*, *52*, 102336. Retrieved from `https://www.sciencedirect.com/science/article/pii/S2352485522000901` doi: https://doi.org/10.1016/j.rsma.2022.102336

Chao, S.-Y., Kao, T. W., & Al-Hajri, K. R. (1992). A numerical investigation of circulation in the arabian gulf. *Journal of Geophysical Research: Oceans*, *97*, 11219-11236.

Egbert, G. D., Bennett, A. F., & Foreman, M. G. G. (1994). Topex/poseidon tides estimated using a global inverse model. *Journal of Geophysical Research: Oceans*, *99*, 24821-24852.

Egbert, G. D., & Erofeeva, S. Y. (2002). Efficient inverse modeling of barotropic ocean tides. *Journal of Atmospheric and Oceanic Technology*, *19*, 183-204.

Emery, K. O. (1956). Sediments and water of Persian Gulf. *AAPG Bulletin*, *40*(10), 2354–2383.

Farmer, D. M., & Armi, L. (1986). Maximal two-layer exchange over a sill and through the combination of a sill and contraction with barotropic flow. *Journal of Fluid Mechanics*. doi: 10.1017/S002211208600246X

Field, C. B., & Barros, V. R. (2014). *Climate change 2014–impacts, adaptation and vulnerability: Regional aspects*. Cambridge University Press.

Hughes, P., & Hunter, J. R. (1979). A proposal for a physical oceanography program and numerical modeling of the kap region. *UNESCO Rep. Mar. Sci*, *27*.

Hunter, J. R. (1983). A review of the residual circulation and mixing processes in the kuwait action plan region, with reference to applicable modelling techniques. In (p. 37-45).

Hyder, P., While, J., Arnold, A., O'Dea, E., Furner, R., Siddorn, J., ... Sykes, P. (2013). Evaluating a new nemo-based Persian/Arabian Gulf tidal operational model. *Journal of Operational Oceanography*, *6*, 3-16. doi: 10.1080/1755876X.2013.11020140

Jain, V., Shankar, D., Vinayachandran, P., Kankonkar, A., Chatterjee, A., Amol, P., ... others (2017). Evidence for the existence of persian gulf water and Red Sea water in the Bay of Bengal. *Climate dynamics*, *48*(9), 3207–3226.

Jithin, A., & Francis, P. (2020). Role of internal tide mixing in keeping the deep andaman sea warmer than the Bay of Bengal. *Scientific reports*, *10*(1), 1–10.

Johns, W., Yao, F., & Olson, D. (1998). Observations of seasonal exchange through the strait of hormuz. *Oceanography*, *11*(2), 58.

Johns, W., Yao, F., Olson, D., Josey, S., Grist, J., & Smeed, D. (2003). Observations of seasonal exchange through the straits of hormuz and the inferred heat and freshwater budgets of the persian gulf. *Journal of Geophysical Research: Oceans*, *108*(C12).

Kämpf, J., & Sadrinasab, M. (2006). The circulation of the Persian Gulf: a numerical study. *Ocean Science*, *2*(1), 27–41.

Koch-Larrouy, A., Madec, G., Bouruet-Aubertot, P., Gerkema, T., Bessières, L., & Molcard, R. (2007). On the transformation of pacific water into indonesian throughflow water by internal tidal mixing. *Geophysical Research Letters*, *34*(4).

Kurogi, M., & Hasumi, H. (2019). Tidal control of the flow through long, narrow straits: a modeling study for the seto inland sea. *Scientific Reports*. doi: 10.1038/s41598-019-47090-y

Large, W. G., Danabasoglu, G., Doney, S. C., & Mcwilliams, J. C. (1997). Sensitivity to surface forcing and boundary layer mixing in a global ocean model: Annual-mean climatology. *Journal of Physical Oceanography*. doi: 10.1175/1520-0485(1997)027⟨2418:STSFAB⟩2.0.CO;2

Large, W. G., McWilliams, J. C., & Doney, S. C. (1994). Oceanic vertical mixing: A review and a model with a nonlocal boundary layer parameterization. *Reviews of Geophysics*, *32*, 363-403.

Large, W. G., & Nurser, A. G. (2001). Ocean surface water mass transformation. In *International geophysics* (Vol. 77, pp. 317–336). Elsevier.

Lorenz, M., Klingbeil, K., & Burchard, H. (2021). Impact of evaporation and precipitation on estuarine mixing. *Journal of Physical Oceanography*, *51*. doi: 10.1175/jpo-d-20-0158.1

Madah, F., & Gharbi, S. H. (2022). Numerical simulation of tidal hydrodynamics in the arabian gulf. *Oceanologia*, *64*(2), 327–345.

Marshall, J., Adcroft, A., Hill, C., Perelman, L., & Heisey, C. (1997). A finite-volume, incompressible navier stokes model for studies of the ocean on parallel computers. *Journal of Geophysical Research: Oceans*, *102*, 5753-5766.

Mashayekh Poul, H., Backhaus, J., & Huebner, U. (2016). A description of the tides and effect of qeshm canal on that in the Persian Gulf using two-dimensional numerical model. *Arabian Journal of Geosciences*, *9*, 1–11.

McCreary, J. P., Yu, Z., Hood, R. R., Vinaychandran, P., Furue, R., Ishida, A., & Richards, K. J. (2013). Dynamics of the indian-ocean oxygen minimum zones. *Progress in Oceanography*, *112-113*, 15-37. Retrieved from `https://www.sciencedirect.com/science/article/pii/S007966111300027X` doi: https://doi.org/10.1016/j.pocean.2013.03.002

Nagai, T., & Hibiya, T. (2015). Internal tides and associated vertical mixing in the i ndonesian a rchipelago. *Journal of Geophysical Research: Oceans*, *120*(5), 3373–3390.

Naranjo, C., Garcia-Lafuente, J., Sannino, G., & Sanchez-Garrido, J. C. (2014). How much do tides affect the circulation of the mediterranean sea? from local processes in the strait of gibraltar to basin-scale effects. *Progress in Oceanography*. doi: 10.1016/j.pocean.2014.06.005

Noori, R., Tian, F., Berndtsson, R., Abbasi, M. R., Naseh, M. V., Modabberi, A., ... Kløve, B. (2019). Recent and future trends in sea surface temperature across the Persian Gulf and Gulf of Oman. *PloS one*, *14*(2), e0212790.

Paparella, F., D'Agostino, D., & A. Burt, J. (2022). Long-term, basin-scale salinity impacts from desalination in the Arabian/Persian Gulf. *Scientific reports*, *12*(1), 20549.

Poul, H. M., Backhaus, J., Dehghani, A., & Huebner, U. (2016). Effect of subseabed salt domes on tidal residual currents in the Persian Gulf. *Journal of Geophysical Research: Oceans*, *121*, 3372-3380.

Pous, Carton, X., & Lazure, P. (2004a). Hydrology and circulation in the strait of hormuz and the gulf of oman-results from the gogp99 experiment: 1. strait of hormuz. *Journal of Geophysical Research C: Oceans*, *109*. doi: 10.1029/2003JC002145

Pous, Carton, X., & Lazure, P. (2004b). Hydrology and circulation in the strait of hormuz and the gulf of omanresults from the gogp99 experiment: 2. gulf of oman. *Journal of Geophysical Research: Oceans*, *109*.

Pous, Carton, X., & Lazure, P. (2012). A process study of the tidal circulation in the persian gulf. *Open Journal of Marine Science*. doi: 10.4236/ojms.2012.24016

Pous, Lazure, P., & Carton, X. (2015). A model of the general circulation in the persian gulf and in the Strait of Hormuz: Intraseasonal to interannual variability. *Continental Shelf Research*, *94*, 55-70.

Privett, D. W. (1959). Monthly charts of evaporation from the n. indian ocean (including the red sea and the persian gulf). *Quarterly Journal of the Royal Meteorological Society*. doi: 10.1002/qj.49708536614

Reynolds, R. M. (1993a). Physical oceanography of the gulf, strait of hormuz, and the gulf of oman-results from the mt mitchell expedition. *Marine Pollution Bulletin*, *27*, 35-59. doi: 10.1016/0025-326X(93)90007-7

Reynolds, R. M. (1993b). Physical oceanography of the gulf, strait of hormuz, and the gulf of omanresults from the mt mitchell expedition. *Marine Pollution Bulletin*, *27*, 35-59.

Rocha, C. B., Chereskin, T. K., Gille, S. T., & Menemenlis, D. (2016). Mesoscale to submesoscale wavenumber spectra in drake passage. *Journal of Physical Oceanography*, *46*, 601-620.

Sannino, G., Bargagli, A., & Artale, V. (2004). Numerical modeling of the semidiurnal tidal exchange through the strait of gibraltar. *Journal of Geophysical Research C: Oceans*. doi: 10.1029/2003JC002057

Sannino, G., Carillo, A., Pisacane, G., & Naranjo, C. (2015). On the relevance of tidal forcing in modelling the mediterranean thermohaline circulation. *Progress in Oceanography*, *134*, 304-329. Retrieved from `http://dx.doi.org/10.1016/`

484 j.pocean.2015.03.002 doi: 10.1016/j.pocean.2015.03.002
485 Sheehan, P. M., Webber, B. G., Sanchez-Franks, A., Matthews, A. J., Heywood,
486 K. J., & Vinayachandran, P. (2020). Injection of oxygenated persian gulf
487 water into the southern Bay of Bengal. *Geophysical Research Letters*, *47*(14),
488 e2020GL087773.
489 Smith, W. H. F., & Sandwell, D. T. (1997). Global sea floor topography from satel-
490 lite altimetry and ship depth soundings. *Science*, *277*, 1956-1962.
491 Swift, S. A., & Bower, A. S. (2003). Formation and circulation of dense water in
492 the persian/arabian gulf. *Journal of Geophysical Research C: Oceans*. doi: 10
493 .1029/2002jc001360
494 Thoppil, P. G., & Hogan, P. J. (2010a). persian gulf response to a wintertime
495 shamal wind event. *Deep-Sea Research Part I: Oceanographic Research Papers*,
496 *57*, 946-955. doi: 10.1016/j.dsr.2010.03.002
497 Thoppil, P. G., & Hogan, P. J. (2010b). Persian Gulf response to a wintertime
498 shamal wind event. *Deep Sea Research Part I: Oceanographic Research Papers*,
499 *57*, 946-955.
500 Vasou, P., Vervatis, V., Krokos, G., Hoteit, I., & Sofianos, S. (2020). Variability of
501 water exchanges through the strait of hormuz. *Ocean Dynamics*, *70*(8), 1053–
502 1065.
503 Wang, X., Peng, S., Liu, Z., Huang, R. X., Qian, Y.-K., & Li, Y. (2015). Tidal mix-
504 ing in the south china sea: An estimate based on the internal tide energetics.
505 *Journal of Physical Oceanography*, *46*, 107-124. doi: 10.1175/jpo-d-15-0082.1
506 Xue, P., & Eltahir, E. A. (2015). Estimation of the heat and water budgets of the
507 persian (arabian) gulf using a regional climate model. *Journal of Climate*,
508 *28*(13), 5041–5062.
509 Yao, F., & Johns, W. E. (2010). A hycom modeling study of the persian gulf: 1.
510 model configurations and surface circulation. *Journal of Geophysical Research:*
511 *Oceans*. doi: 10.1029/2009JC005781

512

513

514

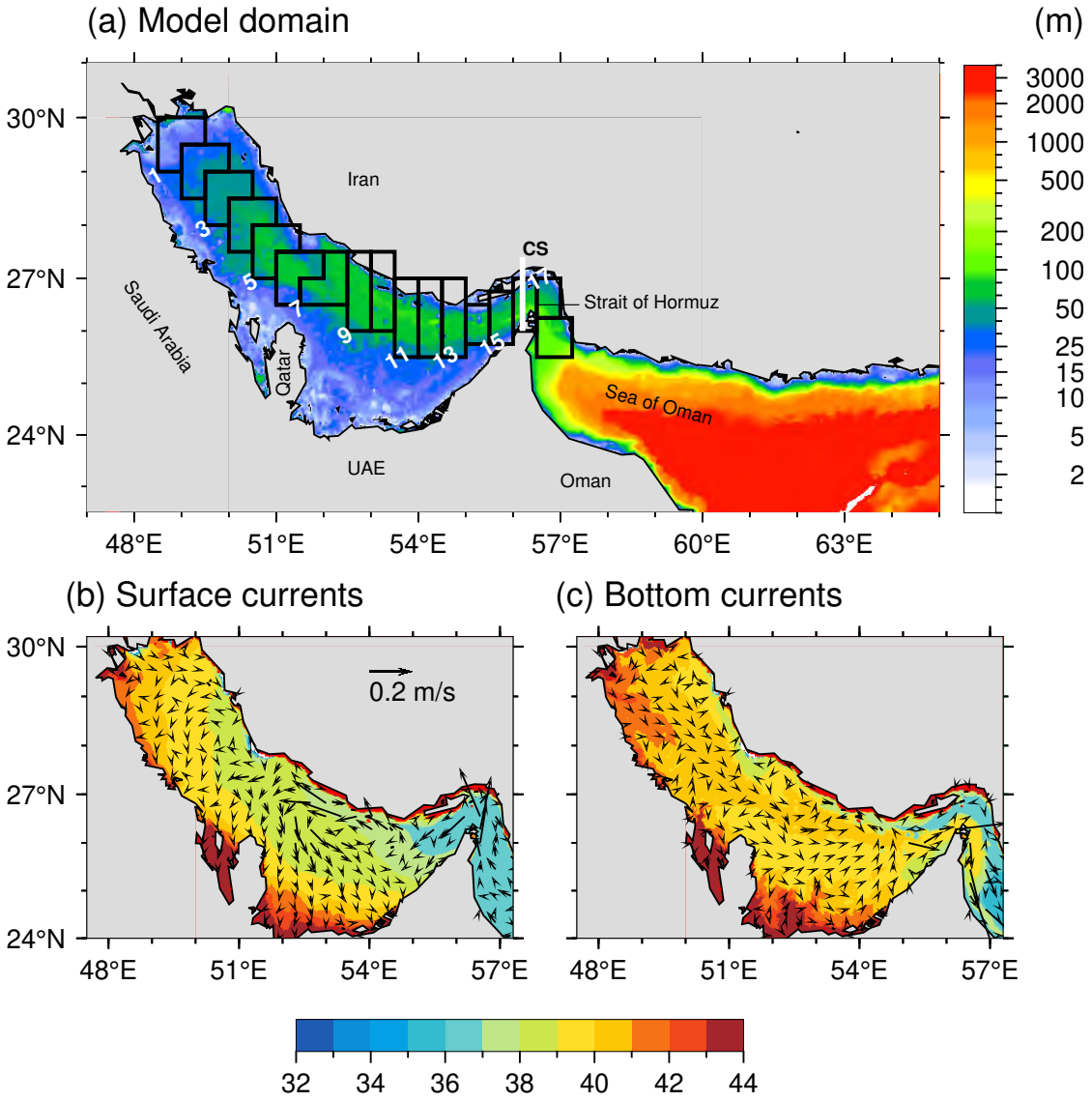

Figure 1: (a) Bathymetry of the study area (color scale in meters) together with the locations of 18 geographical regions — marked by the black boxes — adopted from the observational study of Swift and Bower (2003). Our numerical model is compared as a function of depth with horizontal averages of in situ observations within each box. The cross-section (CS), through which the inflow, outflow and exchange are calculated in the proximity of the Strait of Hormuz, is marked by the thick white line. (b,c) Annual average of surface and bottom current with the salinity (in psu) — scale at the bottom — shown in color. A reference vector showing the velocity scale is also marked.

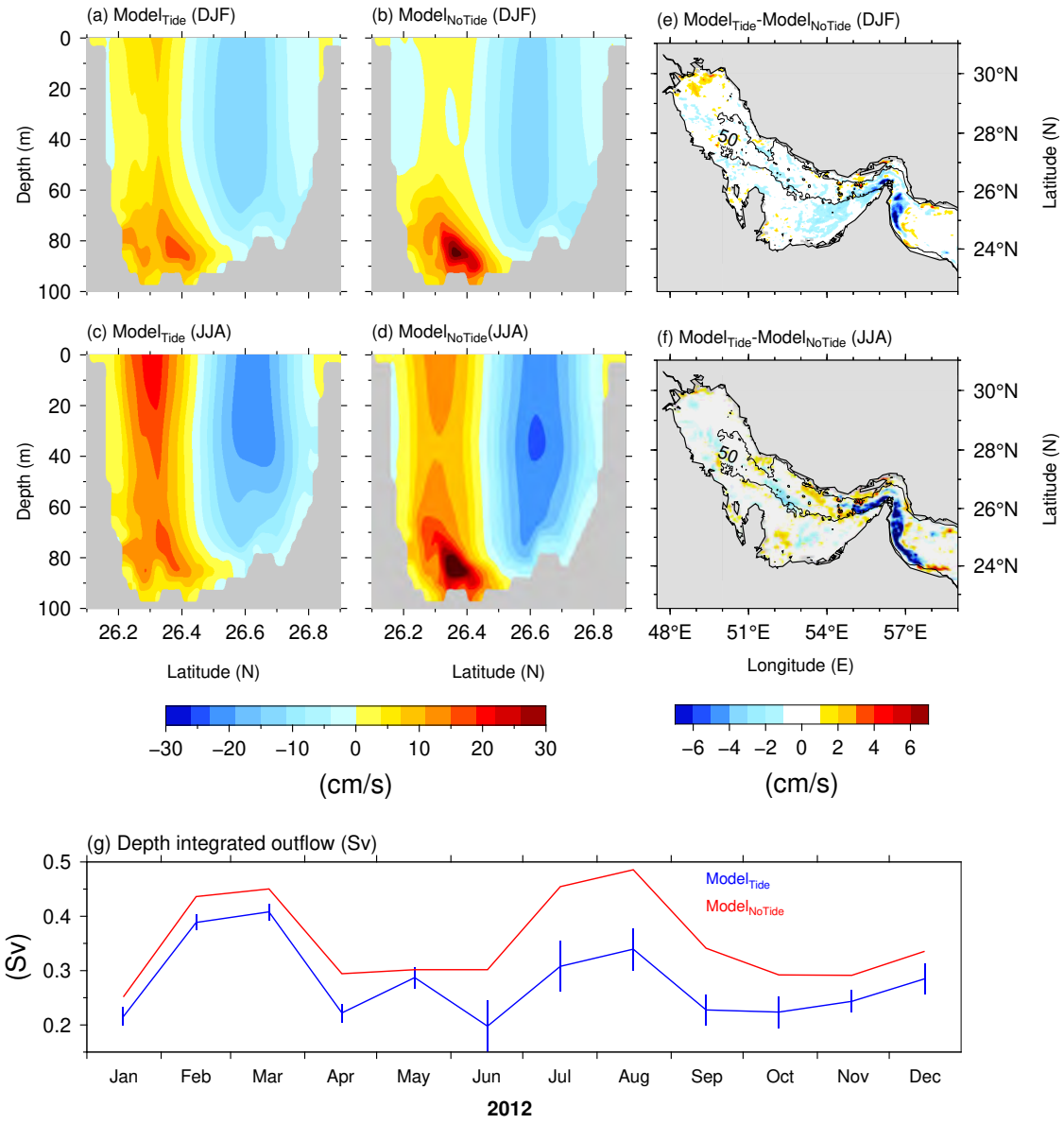

Figure 2: Seasonal average of model currents across the section CS (marked by the thick white line in Figure 1) with (left column) and without (middle column) tidal forcing: (a,b) show winter and (c,d) summer. The difference in bottom currents between simulations with and without tidal forcing during (e) winter and (f) summer. The color scale is in cm/s. (g) Monthly averaged volume transport (in Sverdrups) across CS, close to the Strait of Hormuz, estimated from simulations with (blue) and without (red) tidal forcing. The monthly standard deviation in transport during 2003-2018 including tides is indicated by the vertical bars. Positive values represent transport out of the Gulf.

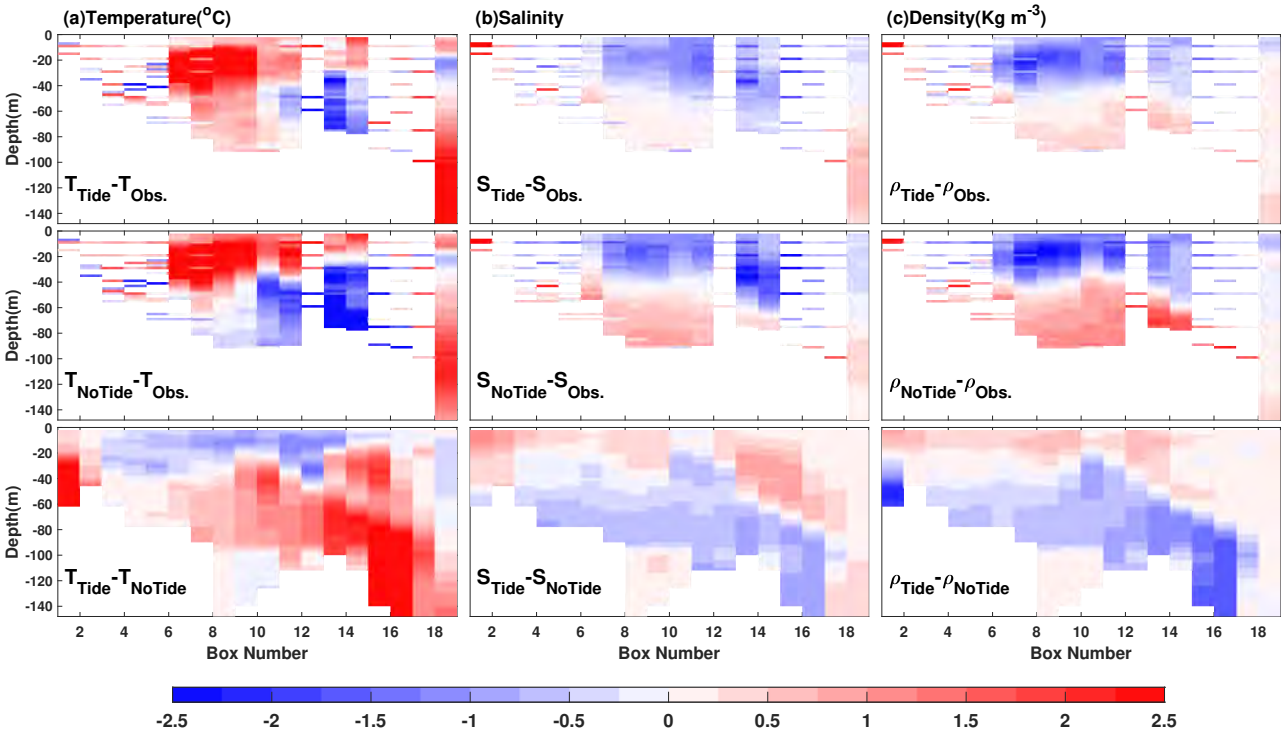

Figure 3: Comparison of summertime model solution with observations averaged over the 18 black boxes marked in Fig.1, plotted as a function of depth and box number. The box number increases moving eastward from the western-most box. Summertime differences in (a) temperature, (b) salinity and (c) density between the model solution with tides (labeled tide) and without tide (notide) and observations (MOODS) (Alessi et al., 1999). The bottom row of panels shows the summertime difference between the model with tides and without tides. The scale at the bottom is common to all plots.

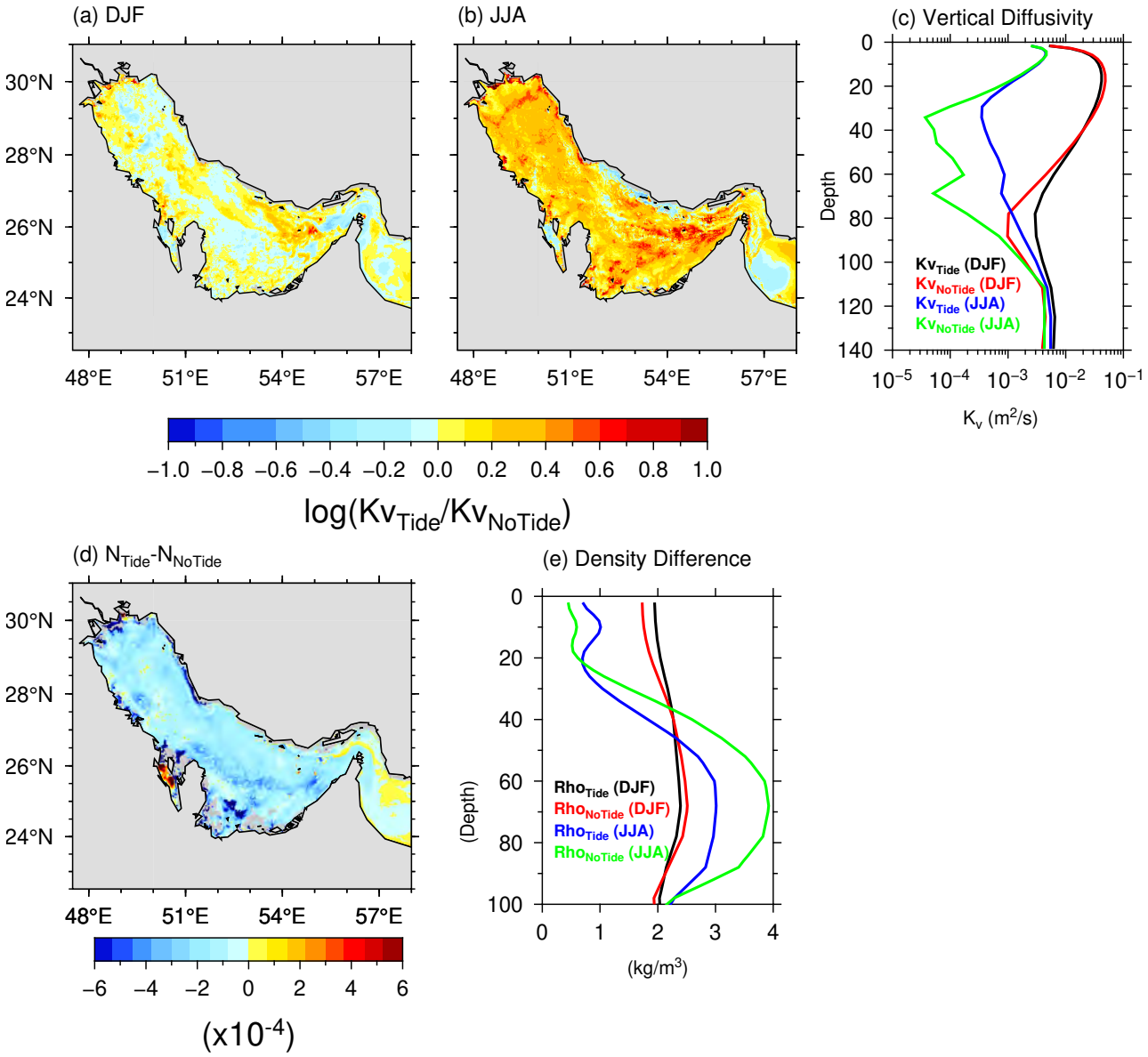

Figure 4: Depth-averaged spatial maps of vertical mixing ratio between tide and no-tide simulations using a logarithmic scale during (a) winter (DJF) and (b) summer (JJA). (c) Vertical profiles of spatially averaged vertical mixing (logarithmic scale) from simulations with and without tides during winter (DJF) and summer (JJA). (d) Difference between depth-averaged stratification, N, with and without tidal forcing during summer (JJA). (e) The vertical variation of density difference between AG (average of boxes 10,11 & 12) and the Sea of Oman (average of boxes 17 & 18) during winter (DJF) and Summer (JJA).

Supplementary: Role of tidal mixing on ocean exchange through the Strait of Hormuz

Mohammed Salim[1,2], Subeesh M. P.[1,3,4], Jeffery Scott[5], Hajoon Song[6,7], John Marshall[5], and Maryam R. Al Shehhi[1]*

[1]Department of Civil Infrastructure and Environmental Engineering, Khalifa University of Science and Technology, Abu Dhabi, United Arab Emirates
[2]Department of Meteorology, University of Reading, UK.
[3]MARUM – Center for Marine Environmental Science, University of Bremen, Bremen, Germany
[4]Institute of Environmental Physics, University of Bremen, Bremen, Germany
[5]Earth, Atmospheric and Planetary Science Department, Massachusetts Institute of Technology, 77 Massachusetts Ave., Cambridge, MA 02139, USA.
[6]Department of Atmospheric Sciences, Yonsei University, Seoul, Korea
[7]Division of Environmental Science & Engineering, Pohang University of Science and Technology, Pohang, Republic of Korea

Corresponding author: Maryam R. Al Shehhi, maryamr.alshehhi@ku.ac.ae

1 Comparison of model with observations

1.1 Tidal elevation

Model performance to simulate tides is evaluated through comparison with major tidal constituents (M2, S2, K1 and O1) at 37 tide gauge stations distributed over the Gulf and Sea of Oman shown in Fig. S1. The tide gauge data are obtained from the International Hydrographic Office and published by Pous et al. (2012). Fig. S2 shows M2, S2, K1 and O1 extracted from MITgcm versus the observed data. Close agreement between the model and observed tidal elevations and phases is found. The corresponding correlation (R2) values between modelled and observed tidal amplitudes are encouraging with values of 0.82, 0.84, 0.62, and 0.80, respectively. Similarly, high R2 values are found between the modelled and observed tidal phases (0.92, 0.91, 0.93 and 0.96), for M2, S2, K1 and O1. In addition, the model is able to reproduce the amphidromic points caused by the diurnal and semidiurnal tidal constituents (Figure S5) . To further quantitatively assess predicted tidal amplitudes, the root mean square error (RMSE) for each tidal constituent at each coastal tide-gauge station is estimated as follows:

$$RMSE = \sqrt{\frac{1}{T}(A_o \cos(\omega t - \phi_o) - A_m \cos(\omega t - \phi_m))} \tag{1}$$

where A and ϕ are the amplitude and phase respectively obtained from observed and modelled tidal levels and T is the length of the time sample. The model shows good agreement with the observations in both the Arabian Gulf and the Sea of Oman. The average RMSE values for tidal levels at M2, S2, K1 and O1 are 13.5, 8.08, 6 and 4.8cm, respectively. The RMSE of M2 is a maximum of 15cm or so at the 4 stations near Qatar and Bahrain where the water is very shallow. However, elsewhere in the Gulf, the RMSE does not exceed 10cm.

The spatial distribution of the amplitudes and phases of modelled tidal components M2, S2, K1 and O1 are shown in Figure S5, and are consistent with the findings of Pous et al. (2012), Madah and Gharbi (2022), Hyder et al. (2013) and Mashayekh Poul et al. (2016). As can be seen, the most notable tidal feature are: (i) highest amplitudes of M2, S2 and K1 in the Strait of Hormuz, and (ii) the presence of mixed semi-diurnal and diurnal tides in the Gulf. There are two amphidromic points caused by the semi-diurnal tides: one in the south-eastern region of the Gulf near the coast of Abu Dhabi and the other in the south-western side of the Gulf. In contrast, there is an amphidromic point caused by diurnal tides in the south-central region of the Gulf off the coast of Bahrain. Based on these patterns, the M2 tide is the most dominant constituent throughout the Gulf and Sea of Oman, followed by K1, S2 and O1. The M2 tide reaches a maximum amplitude of 149 cm in strongly shoaling and narrowing regions such as the north-western end of the Gulf and near the Iranian coastal region off the Strait of Hormuz. Similarly, K1 dominates over S2 in most of the Gulf, except the areas surrounding the Strait of Hormuz and the diurnal amphidromic point. A maximum K1 amplitude of 48 cm is observed on the western coast of UAE (Abu Dhabi) near Qatar and on the eastern side of the UAE adjacent to the Omani coastal area of the Sea of Oman. The S2 tide reaches a maximum value of 68 cm on the Iranian coast off Hormuz strait. The diurnal component O1 follows the pattern of K1 but has a maximum value of 27 cm.

1.2 Tidal currents

Instantaneous ocean currents u and v are compared with time series data obtained from five mooring stations are plotted in Figure S3 and S4 (Reynolds, 1993) at different depths (10m, 15m, 21m, 24m, 30m, 40m, 56m and 84m). The skill of the model is measured using Willmott's method (Willmott, 1981) as described by Warner et al. (2005). Skill values vary from 0, indicating complete disagreement, to 1, perfect agreement, be-

tween model and observation thus:

$$skill = 1 - \frac{\Sigma_{i=1}^{n}|Y_m - Y_o|^2}{\Sigma_{i=1}^{n}(|Y_m - (Y_o)| + |Y_o - (Y_o)|)^2}. \quad (2)$$

The average model skill value at all mooring locations (MB2, MB3, MB4, MB5 and MB7) with different depth levels was 0.7 for both u and v (Figure S4). The lowest skill values of 0.5-0.6 for the v component are found at mooring MB2. The tidal current analysis at MB2 shows that it is dominated by tidal currents. The maximum simulated u and v values of the 10 m current are 22.7 cms^{-1} and 6 cms^{-1}, respectively, in good agreement with the observations (22.6 cms^{-1} and 6.49 cms^{-1}). The magnitudes of the currents decrease with depth. For example, at 40 m the simulated u and v components at MB2 are 14 and 10.1 cms^{-1}, respectively, which are close to the observed values of 13 cms^{-1} and 8.6 cms^{-1}.

References

Hyder, P., While, J., Arnold, A., O'Dea, E., Furner, R., Siddorn, J., ... Sykes, P. (2013). Evaluating a new nemo-based Persian/Arabian Gulf tidal operational model. *Journal of Operational Oceanography*, *6*, 3-16. doi: 10.1080/1755876X.2013.11020140

Madah, F., & Gharbi, S. H. (2022). Numerical simulation of tidal hydrodynamics in the arabian gulf. *Oceanologia*, *64*(2), 327–345.

Mashayekh Poul, H., Backhaus, J., & Huebner, U. (2016). A description of the tides and effect of qeshm canal on that in the Persian Gulf using two-dimensional numerical model. *Arabian Journal of Geosciences*, *9*, 1–11.

Pous, Carton, X., & Lazure, P. (2012). A process study of the tidal circulation in the persian gulf. *Open Journal of Marine Science*. doi: 10.4236/ojms.2012.24016

Reynolds, R. M. (1993). Physical oceanography of the gulf, strait of hormuz, and the gulf of omanresults from the mt mitchell expedition. *Marine Pollution Bulletin*, *27*, 35-59.

Warner, J. C., Sherwood, C. R., Arango, H. G., & Signell, R. P. (2005). Performance of four turbulence closure models implemented using a generic length scale method. *Ocean Modelling*, *8*, 81-113. doi: 10.1016/j.ocemod.2003.12.003

Willmott, C. J. (1981). On the validation of models. *Physical Geography*. doi: 10.1080/02723646.1981.10642213

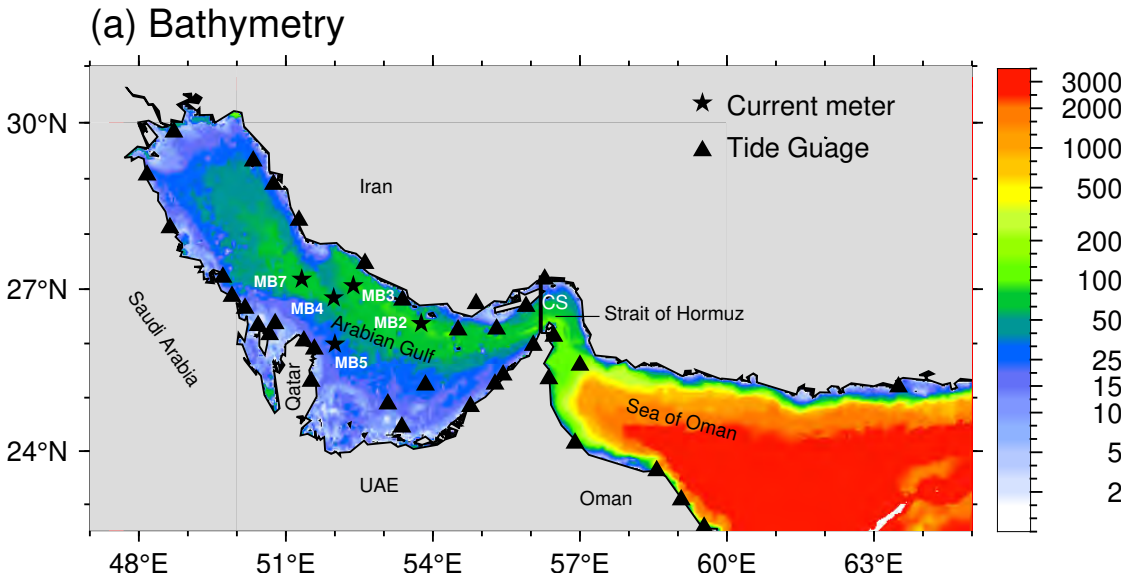

Figure S1: The bathymetry of the Arabian Gulf. The black triangles mark the location of tide gauges. The location of current meter moorings are marked by stars. The section across the Strait is also shown.

93

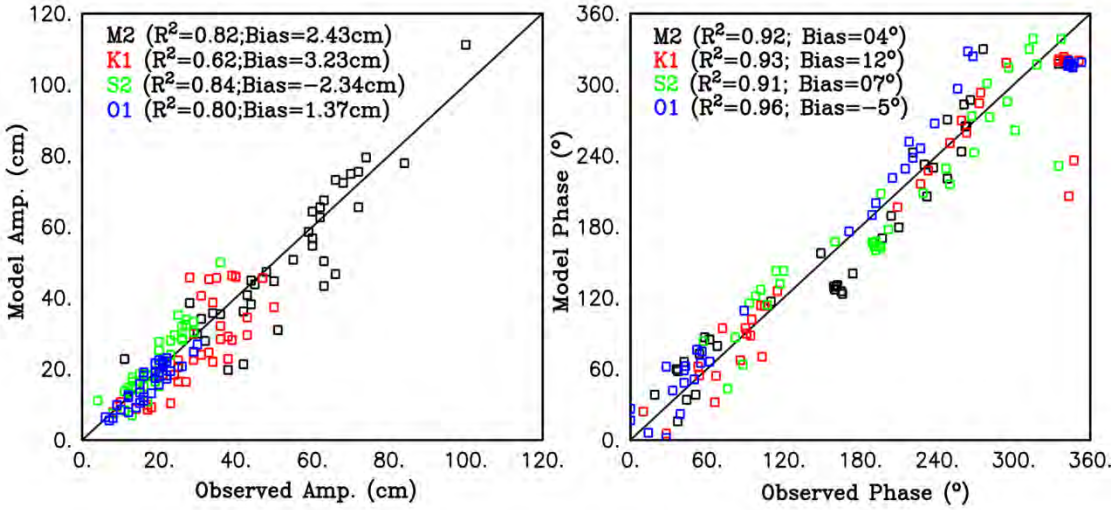

Figure S2: Observed vs model amplitude and phases of major tidal constituents (M2, S2, K1, O1) at the position of tide guages: color coding is black, red, green and blue squares for the M2, K1, S2 and O1 tidal constituents respectively.

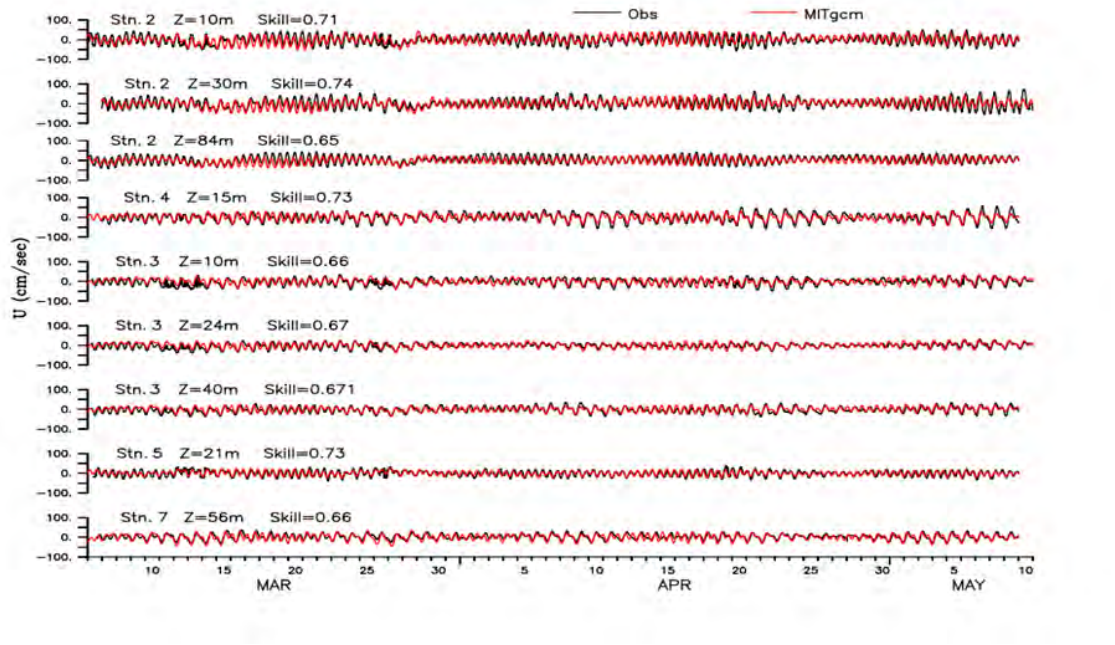

Figure S3: Comparison of modeled and observed zonal currents at chosen mooring locations and depths. The solid black line represents the observed currents and red lines are extracted from the model at corresponding locations.

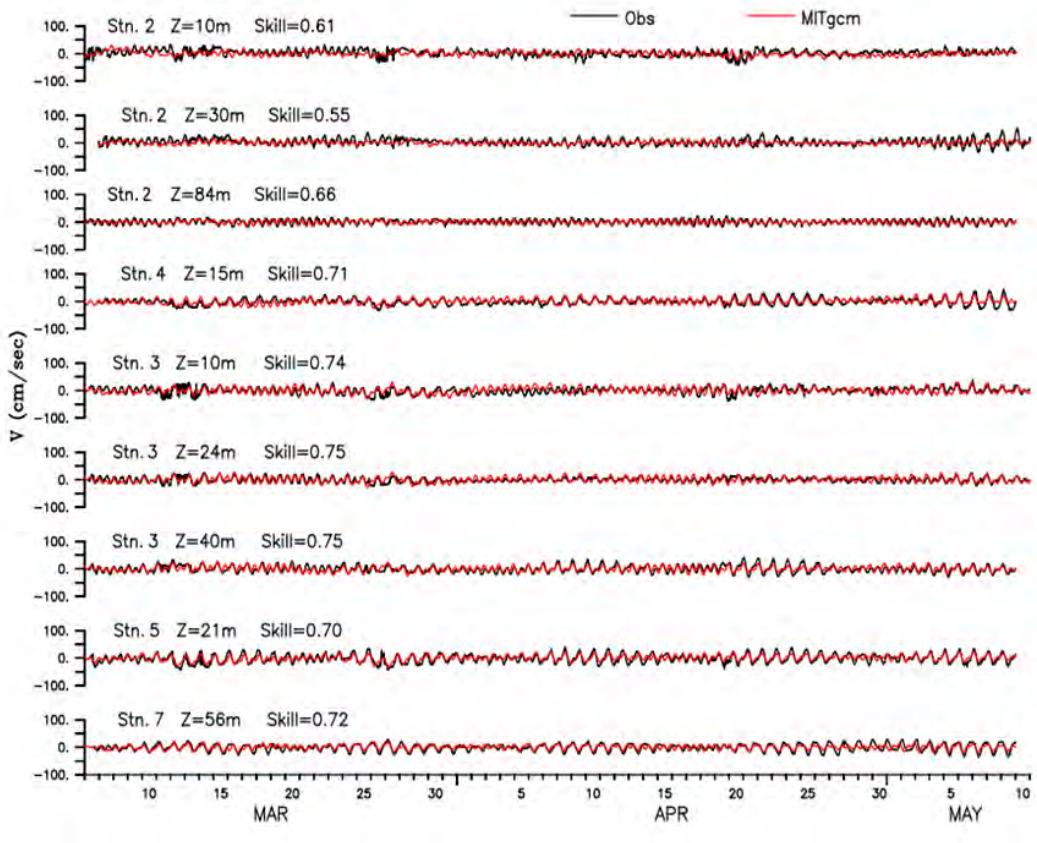

Figure S4: Comparison of modeled and observed meridional currents at chosen mooring locations and depths. The solid black line represents the observed currents and red lines are extracted from the model at corresponding locations. The scale of the vectors is indicated by the arrow at the top right.

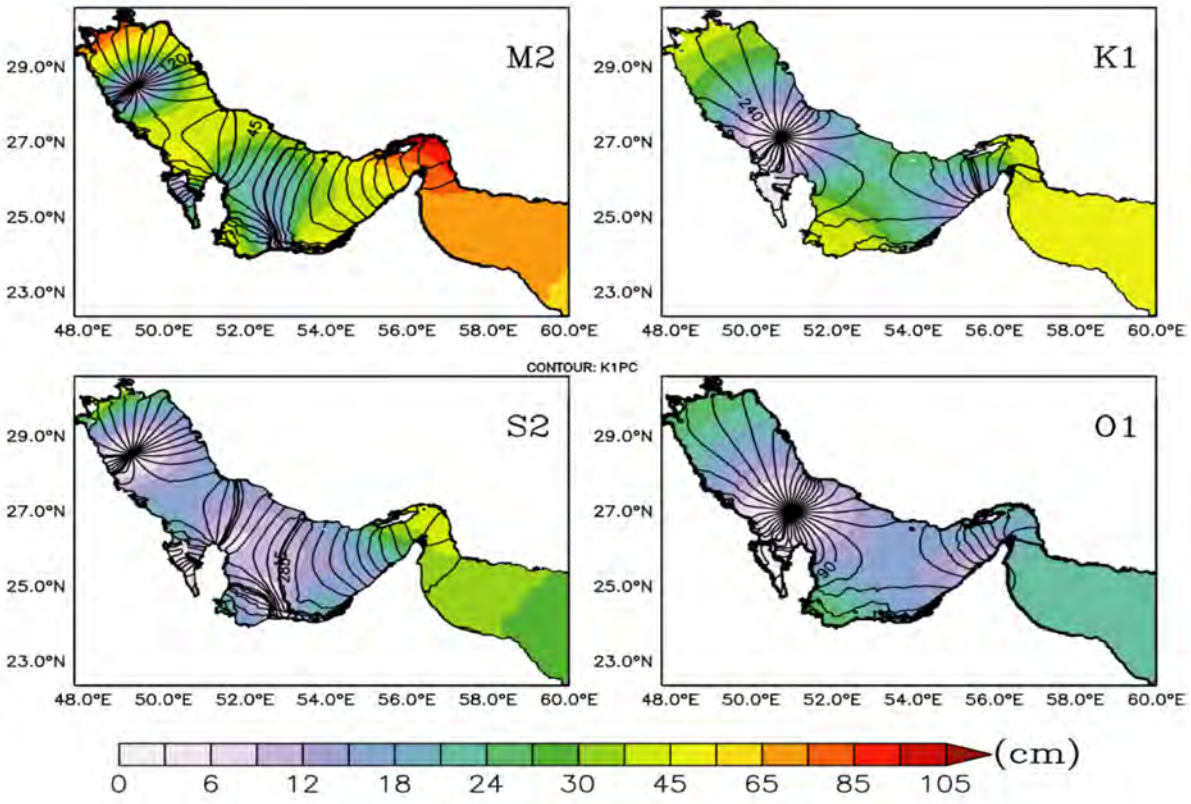

Figure S5: Co-Tidal chart for M2, S2, K1 and O1. Model derived amplitudes in cm (shaded in colors) overlaid with phase contours of major tidal constituents (M2, S2, K1 and O1).

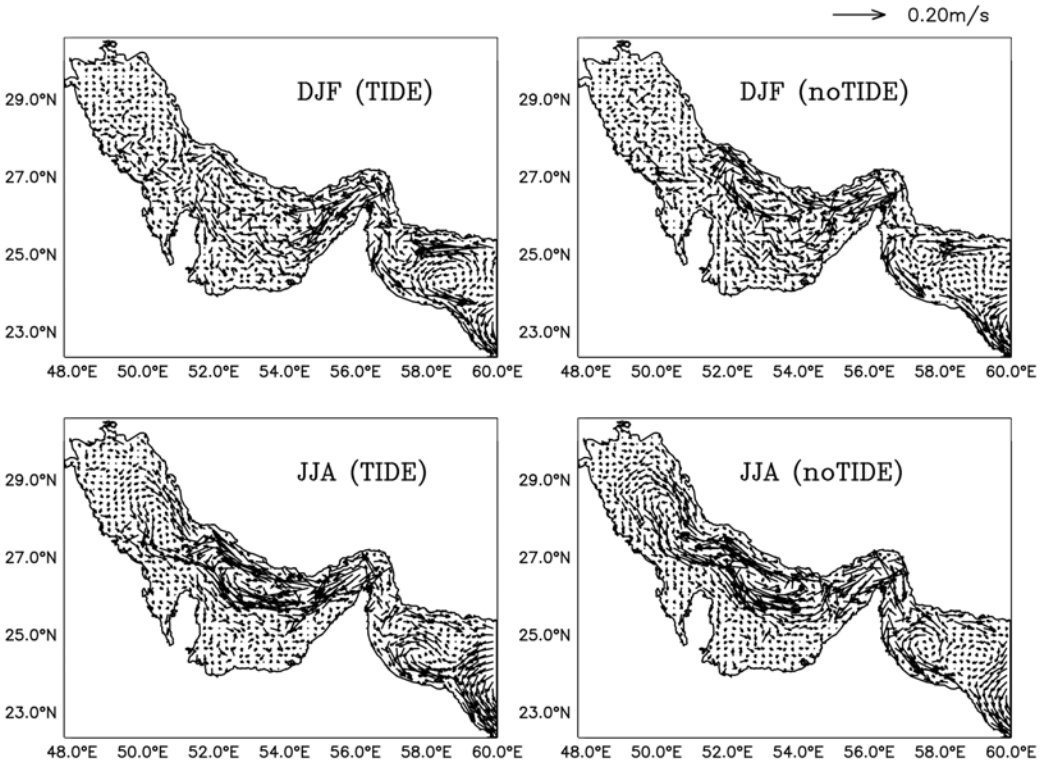

Figure S6: The panels on the left show modeled depth-averaged current vectors with tides during (top) winter and (bottom) summer. The panels on the right panel show the same but in the case of no tides. The scale of the vector is indicated at the top.

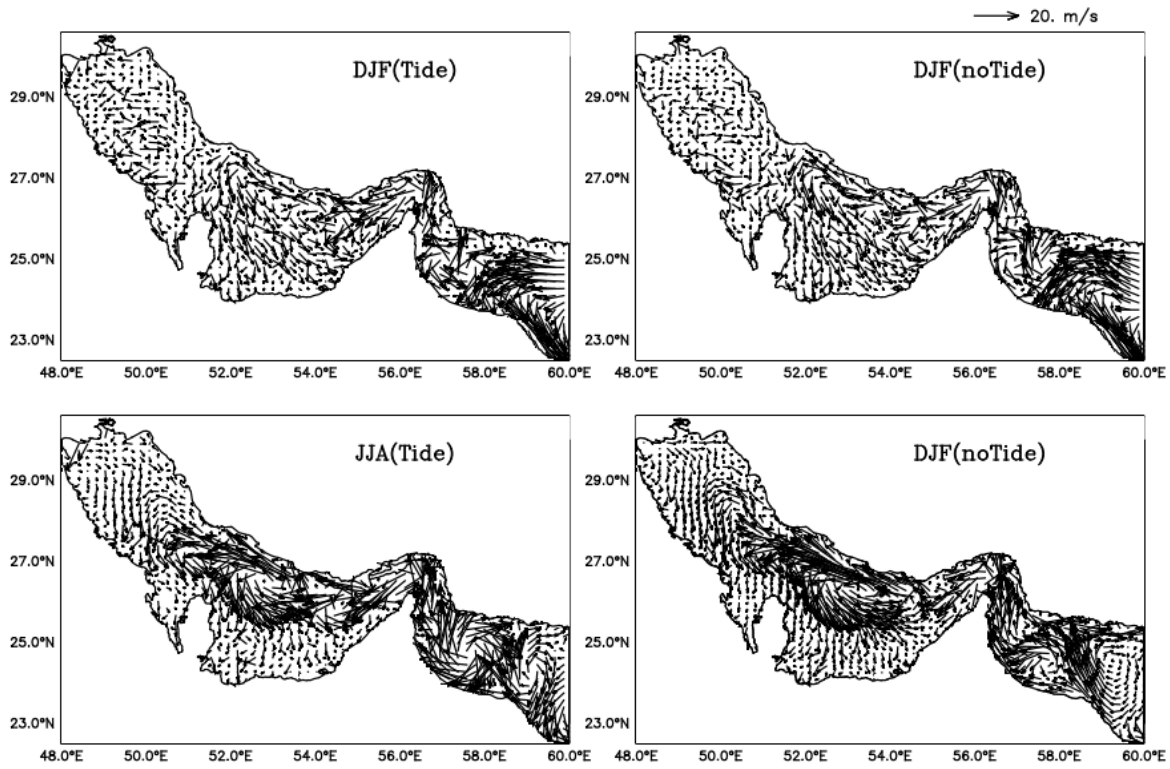

Figure S7: The panels on the left show modeled surface current vectors in m/s with tides during (top) winter and (bottom) summer. The panels on the right panel show the same but in the case of no tides. The scale of the vector is indicated at the top.

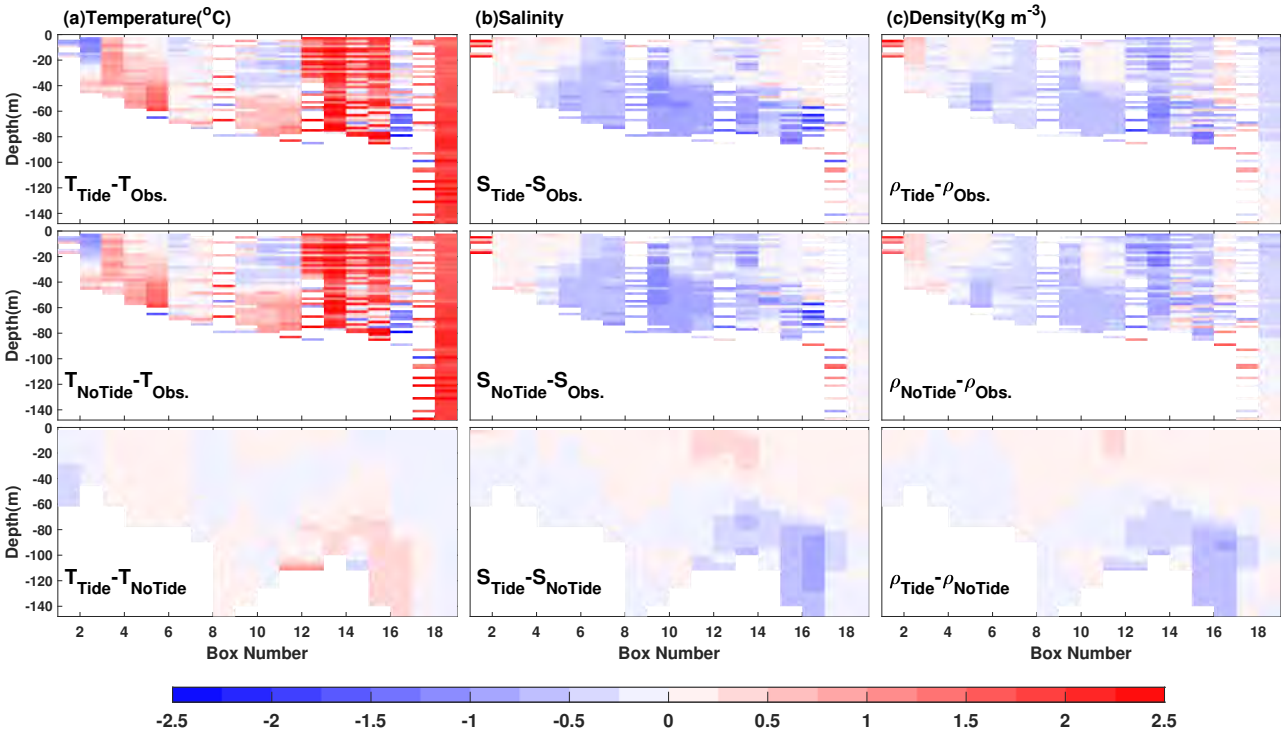

Figure S8: Comparison of wintertime model solution with observations averaged over the 18 black boxes marked in Fig.1, plotted as a function of depth and box number. The box number increases moving eastward from the western-most box. Wintertime differences in (a) temperature, (b) salinity and (c) density between the model solution with tides (labeled tide) and without tide (notide) and observations (MOODS) (Alessi et al. 1999). The bottom row of panels shows the wintertime difference between the model with tides and without tides. The scale at the bottom is common to all plots.

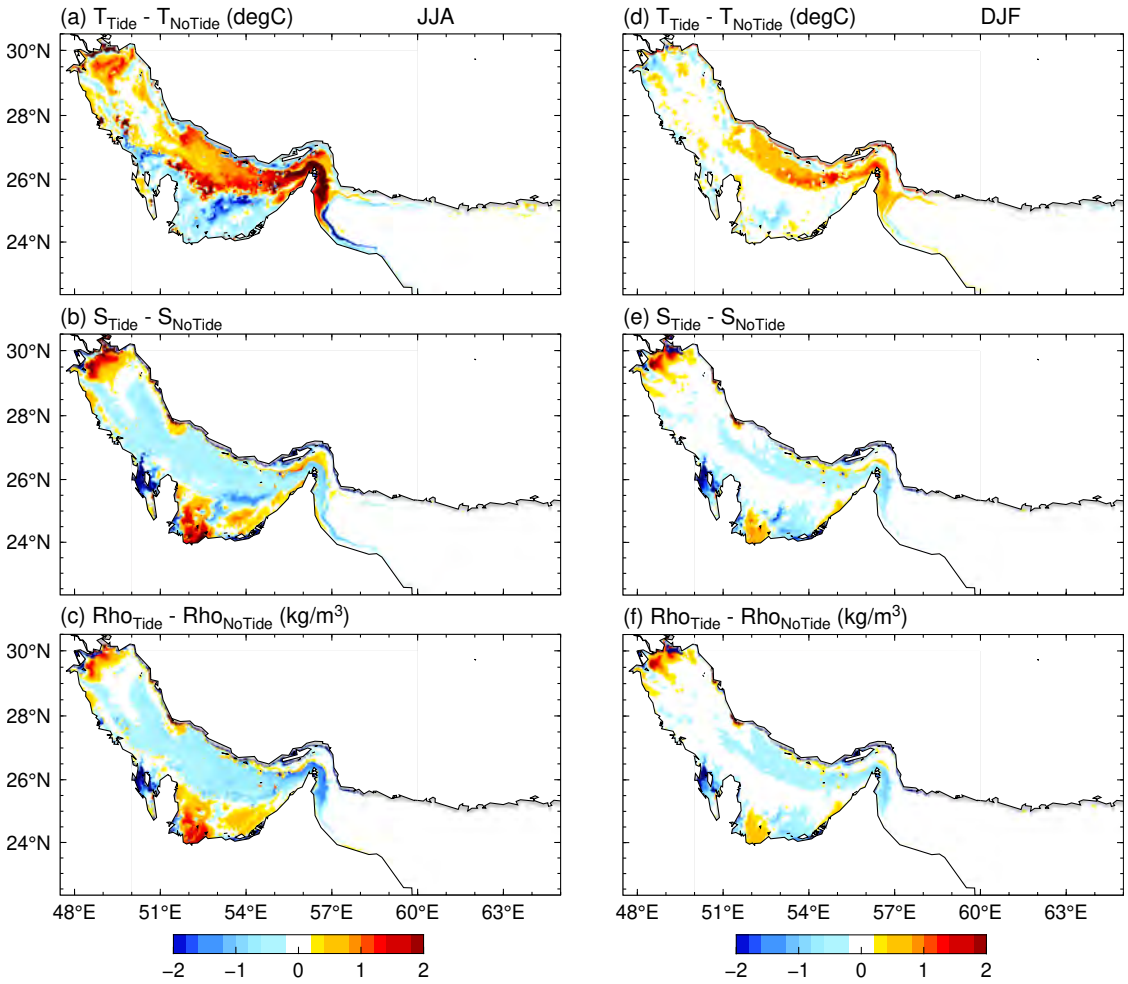

Figure S9: Differences between simulations with tide and without tide at the bottom of the model: (a) Temperature, (b) Salinity, (c) Density in JJA; (d), (e), and (f) show the same parameters during DJF.